RJC

RASĀYAN *J. Chem.*
Vol. 18 | No. 3 |1620-1634| July-September | 2025
ISSN: 0974-1496 | e-ISSN: 0976-0083 | CODEN: RJCABP
http://www.rasayanjournal.com
http://www.rasayanjournal.co.in

SYNTHESIS AND CHARACTERIZATION OF Ag: NiO NANO COMPOSITE VIA GREEN ROUTE FOR PHOTOCATALYTIC AND SUPERCAPACITOR APPLICATIONS

Ramasubbaiah Vusenappagari✉ and Behara Dilip Kumar
Department of Chemical Engineering, JNTUA College of Engineering, Ananthapuramu, Andhra Pradesh 515002, India
✉Corresponding author: ramasubbaiah.v@gmail.com

ABSTRACT

In the present research work, an Ag: NiO nanocomposite was synthesized through a biomediated solution combustion method using Tulsi leaf extract. The confirmation of the Composite material was done by XRD, DRS, SEM, EDAX, TEM, and TGA spectral methods. The XRD reveals that the average crystallite size of Ag: NiO NC is ~ 30 nm. The SEM clearly shows a hexagonal shape and an average particle size of about 85 nm. The TEM images show that Ag diffraction spots typically correspond to the FCC structure, while NiO shows diffraction rings/spots consistent with its cubic structure. The energy band gap value for Ag: NiO NC of 3.84 eV is confirmed by DRS spectra. The TGA shows good heat stability and 90.81% of residue formation with a calcination temperature of Ag: NiO NPs developed even after 400 °C. The prepared composite was used for the photodegradation of Fast Orange Red (FOR), showing a maximum absorption at 495 nm with 74.59% degradation under UV light irradiation. The Ag: NiO NC was also used for Cyclic Voltammetric (CV) studies, exhibiting a surface redox mechanism of Ni^{2+} to Ni^{3+}, which emerged at -0.01 V (cathodic) and -0.30 V (anodic) at 10 mV/s in 1 M KOH solution. The GCD shows good specific capacitances of 380.4 F/g at a current density of 5 A/g. The Ag: NiO NC shows outstanding cycle stability, retaining 94.5% of its starting value after 3000 cycles. This suggests that the electrode is appropriate for use in supercapacitors.

Keywords: Ag: NiO NC, FOR, Photodegradation, Supercapacitor, Specific Capacitance, Solution Combustion
RASĀYAN *J. Chem.*, Vol. 18, No. 3, 2025

INTRODUCTION

The discharge of particular industrial pollutants like drugs, paint, textiles, leather, food, and so many other industries toxic materials to the aquatic environment has demanding the importance of control, monitoring, and removal of these toxic materials due to their non-biodegradable behavior, they cause a variety of illnesses that affect the entire biota. To provide a safe and healthy atmosphere, organic effluents must be removed.[1] Photocatalysis, which aims to produce an affordable and environmentally friendly catalyst with adequate mineralization capability, has been increasingly popular in recent decades, especially in addressing energy and pollution issues.[2] Since the mineralization process is typically not allowed by the bandgaps of the various semiconductors, its applications are comparatively limited. Therefore, by altering the semiconductors, new types of photocatalysts having significant activity in the presence of UV light must be developed. Several forms of metal oxides, including TiO_2, Co_3O_4, AgO, and NiO, have been employed for the photochemical mineralization of hazardous substances throughout the past few decades.[3,10] All of these photocatalysts do, however, have significant drawbacks, such as (i) reduced light transmittance, (ii) nanoparticle aggregation, and (iii) reduced surface area. Therefore, additional synthesis innovation is needed to improve the photocatalytic efficiency. The organic dye pollutants cause various health disorders in human beings and mainly affect the central nervous system, the brain, and the liver due to their persistent toxicity and non-biodegradability.[11] Therefore, it is necessary that wastewater effluents containing dyes be treated immediately before being released into the environment. Fast Orange Red is a synthetic dye commonly used in textiles and biological staining, particularly in histology.[12] Like many azo dyes, it is known for its vibrant color and ability to bind to various materials. However, Fast Orange Red and similar dyes can pose environmental challenges due to

http://doi.org/10.31788/RJC.2025.1839320
This work is licensed under a CC BY 4.0 license.

their persistence in water and soil systems, making their degradation a significant area of interest. Improper disposal of dyes like Fast Orange Red can cause water pollution and affect aquatic animals, and potentially affect humans due to their toxic and carcinogenic breakdown products. Therefore, developing effective degradation methods is essential for reducing their environmental impact. Various technological facets are being investigated in the vast field of nanoscience. Over the past few decades, research has concentrated on nanocomposite (NC) materials since they blend unique features. Supercapacitors and batteries are currently receiving more attention in the creation of new technologies to address energy-related issues.[13,14] Nanocomposites are widely researched in the fields of energy and catalysis because they combine the characteristics of their component materials. The development of high band gap energy (Eg) semiconductors with eminent properties is driven viz TiO_2, ZnO, NiO, SnO_2, etc., which are presently showing more attention due to their large applications.[15,16] Metal oxide (MO) semiconductors are extensively used in various applications, such as emission control, hybrid solar cells, UV shields, LEDs, temperature control paints, gas-sensing devices, photocatalysis, piezoelectric devices, and supercapacitors.[17,24] Semiconducting materials need to be utilized more often in order to restore our damaged atmosphere and sustainably develop technology. The new world of electronic base technologies requires the development of sophisticated electronic characteristics that are both satisfying and advantageous.[25] The supercapacitor is an efficient energy-storage component for the production of high-power appliances in next-generation energy-storage systems.[26] Over the past few years, metal nanostructures have been the subject of numerous studies. Particularly, the combination of metal nanoparticles (MNPs) with oxide systems has drawn attention due to its potential in a variety of fields, such as photocatalysis, sensing, biomedical research, catalysis in different supercapacitors, transformations, etc.[27,28] As a significant metal oxide, NiO has a wide range of uses due to its advantageous qualities, including fuel cell composite anodes, solar cells, gas sensing, electrochromic coatings, dye-sensitized photocathodes, smart windows, energy storage systems, and supercapacitors etc.[29,30] Nickel oxide (NiO) is a semiconductor material characterized by a wide band gap and notable catalytic, optical, and electronic properties. Nickel-based systems exhibit several advantages, including high theoretical capacitance (2584 F/g for NiO), cost-effectiveness, environmental compatibility, excellent chemical and thermal stability, and abundant availability, making them promising candidates for electrode materials. However, NiO faces challenges such as low inherent conductivity, sluggish reaction kinetics, and a limited number of electrochemically active sites, primarily confined to the surface, contributing to its pseudocapacitive behavior. Consequently, exploring strategies to enhance NiO's conductivity using nanocomposite (NC) structures could provide deeper insights into its functional potential.

Silver nanoparticles are also gaining interest because of their numerous scientific and economic uses as well as their special physical, chemical, and biological characteristics, such as their high electrical conductivity.[31,32] Additionally, research has shown that Ag nanostructures have remarkable catalytic properties for reducing organic dyes.[33] Because of their effectiveness and affordability, Ag-NPs have been thoroughly investigated as a catalyst in industrial applications.[34] There have also been reports of studies on Ag NPs improving the electrochemical stability of electrode materials.[35] The previous investigation has examined the impact of Ag loading on graphene-based nanocomposites' supercapacitor performance.[36] Investigating Ag-incorporated NiO systems' electrochemical and catalytic properties would be fascinating. In our present study, we have chosen Ag-NiO (Silver-Nickel Oxide) composites for the photocatalytic and supercapacitor applications due to gaining attention their enhanced photocatalytic and supercapacitor properties compared to their components. Both Ag and NiO contribute to the overall photocatalytic and supercapacitor efficiency by combining their respective strengths.[37,38] NiO is a p-type semiconductor with a band gap ranging from approximately 3.4 to 4.0 eV, primarily enabling light absorption in the UV region. However, its photocatalytic efficiency is hindered by the high recombination rate of electron-hole pairs. Incorporating Ag nanoparticles into NiO can effectively reduce the composite's band gap, enhancing its performance. The surface plasmon resonance (SPR) effect of Ag extends light absorption into the visible spectrum, thereby improving photocatalytic activity under sunlight or visible light. Additionally, in the Ag-NiO composite, a Schottky junction is established between Ag (a metal) and NiO (a semiconductor), which promotes electron transfer from NiO to Ag,

further boosting photocatalytic efficiency. This prevents recombination of electron-hole pairs, allowing more electrons to participate in redox reactions, thus improving photocatalytic efficiency. Ag-NiO composites have demonstrated effective degradation of organic pollutants, including dyes and phenols, due to the synergistic interaction between Ag and NiO. This interaction facilitates the generation of reactive oxygen species (ROS), such as hydroxyl radicals (•OH) and superoxide anions (O_2^-), which play a crucial role in the pollutant degradation process.[39] The Ag-NiO composite shows promising performance as a material for supercapacitors due to its combination of high electrical conductivity from Ag and high pseudocapacitive behavior from NiO.[40] This hybrid structure leverages the strengths of both components, resulting in enhanced electrochemical performance. NiO is known for its excellent pseudocapacitive properties due to redox reactions at the surface of the material. NiO can undergo reversible Faradaic reactions (involving charge transfer), leading to high specific capacitance. Ag nanoparticles enhance the conductivity of the composite by providing efficient electron pathways, which improve the overall charge storage and discharge rates. The incorporation of Ag nanoparticles enhances the specific capacitance of the Ag-NiO composite. While NiO alone exhibits low intrinsic electrical conductivity, which can hinder its performance in supercapacitors, the addition of Ag nanoparticles effectively improves the composite's electrical conductivity, leading to better electrochemical performance. Ag acts as a conductive network that facilitates faster electron transport during charging and discharging, reducing internal resistance (equivalent series resistance, ESR). The synergistic interaction between NiO and Ag results in enhanced charge storage capacity.[41] The high surface area provided by the composite structure, combined with the high electrochemical activity of NiO and the excellent conductivity of Ag, results in faster ion/electron transport and better utilization of active materials.[41] The Ag: NiO nanocomposite was synthesized through a biomediated solution combustion method using Tulsi leaf extract. The confirmation of the Composite material is done by various spectral investigation methods. The photodegradation of Fast Orange Red (FOR) shows a maximum absorption observed at 495 nm with 74.59% degradation under UV light irradiation. The Cyclic Voltammetric (CV) studies exhibit a surface redox mechanism of Ni^{2+} to Ni^{3+}, which emerged at -0.01 V (cathodic) and -0.30 V (anodic) at 10 mV/s using 1 M KOH solution. The GCD confirms good specific capacitances of 380.4 F/g at a current density of 5 A/g. The Ag: NiO NC shows outstanding cycle stability, retaining 94.5% of its starting value after 3000 cycles. This suggests that the electrode is appropriate for use in supercapacitors.

EXPERIMENTAL

Materials

All the Chemicals are obtained from Sigma Aldrich with analytical reagent (A.R.). They are Tulsi leaf, Nickel nitrate ($Ni(NO_3)_2.6H_2O$), Silver Nitrate ($AgNO_3$), Fast Orange Red, 0.1 M KOH, and double-distilled water.

Synthetic Route for the Preparation of Ag-NiO Composite

The Ag: NiO NC was synthesized by burning an extract of Tulsi leaf in a biomediated solution combustion chamber. A magnetic stirrer was used to aggressively mix 1 mL of Tulsi leaf extract with stoichiometric quantities of $Ni(NO_3)_2.6H_2O$ and $AgNO_3$ in a beaker for 10 to 15 minutes, and then placed in a pre-heated muffle furnace at 450 ± 10 °C to get a gel that turns to a white powder. As the reaction commenced within the volume, a flame emerged on the foam's surface and rapidly propagated throughout, resulting in the formation of a white powder with an exceptionally porous structure. Ag-NiO composites were developed using a method that could tolerate high temperatures and self-propagate.[42,43] The whole process was completed in under five minutes. The final products were used for structural and other studies after being further calcined for 3 hours at 600 °C.

Characterization

The structural analysis was conducted using a Shimadzu X-ray diffractometer (CuKα, 1.541 Å) with a scan rate of 2° per minute for PXRD measurements. Functional group identification in the synthesized materials was carried out using a Shimadzu IR Affinity-1S FTIR spectrometer within the 4000–400 cm^{-1} range. The three-dimensional morphology, polycrystallinity, and interplanar spacing were examined using a JEOL JEM-2100 transmission electron microscope (TEM) operating at an accelerating voltage of up to

200 kV with a LaB_6 filament. Diffuse reflectance spectroscopy (DRS) measurements were performed using a Shimadzu UV-Vis spectrophotometer (Model 2600) within the 200 800 nm wavelength range. Electrochemical impedance spectroscopy (EIS) experiments were carried out using a CH Instruments Electrochemical Analyzer (Model 608E) with a three-electrode configuration.

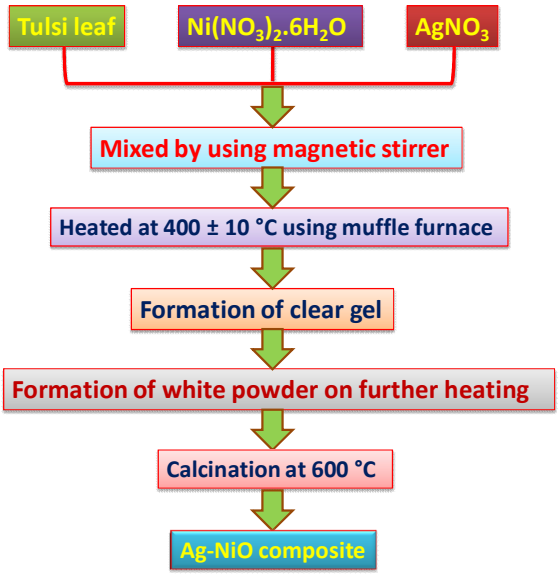

Scheme-1: Schematic Diagram for the Preparation of Ag-NiO Composite

Photocatalytic Analysis

The purpose of the photocatalytic investigation for the developed Ag-NiO composite was to degrade the FOR dye when exposed to ultraviolet light. A 50 mg portion of the photocatalyst was dispersed in 250 mL of a 20 ppm dye solution and exposed to UV light under standard conditions. The Ag: NiO nanocomposite (NC) catalyst was placed in a circular glass reactor. A 400-W mercury vapor (Hg) lamp emitting at 250 nm was used to irradiate the reaction mixture, following magnetic agitation to ensure uniform dispersion. The research was carried out in a Pyrex glass beaker. The resultant mixture was exposed to ultraviolet light in an oxygen atmosphere for 120 minutes. Every 15 minutes during the reaction, 5 mL of the sample solution was extracted, and the UV-visible absorption spectra were recorded in the 200–800 nm range. Ag-NiO composite's photocatalytic activity was evaluated by the degradation of an aqueous solution of FOR[44,45]. The % of degradation was studied by the following eq.-1.

$$\text{Percentage Degradation} = [(C_0-C_e)/C_e] \text{ X100} \quad (1)$$

Where C_0 and C_e are the dye concentrations at times t seconds.

Further, C/Co values were also investigated by eq.- 2.

$$\log(C-C_0) = -K_t \quad (2)$$

Where k is the first-order rate constant. The first-order kinetics was a linear relationship between log C/C_o and K.

Preparation of the Working Electrode

The working electrode was prepared by using graphite powder, prepared nanocomposite, and binder (PTFE) in an agitated mortar in the ratio of 60:20:20%. A paste of composite material is formed. For the enhancement of electrical conductivity, nickel mesh was attached with an active material, and it was compressed for 5 min at 30 MPa. The electrolytic mobility was enhanced by immersing the prepared electrode in a 1 M KOH solution for 40 minutes.[6]

RESULTS AND DISCUSSION

XRD Analysis

X-ray diffraction (XRD) is an effective, non-destructive technique for analyzing the phase composition, crystal structure, and orientation of solid, liquid, and powdered materials. The XRD pattern reveals five distinct peaks at 2θ values of 37.27°, 43.40°, 63.07°, 75.55°, and 79.52°, corresponding to the reflection peaks from the (111), (200), (220), (311), and (222) planes, confirming the formation of cubic crystal NiO (JCPDS card no. 00-047-1049), as shown in Fig.-1. Additionally, Fig.-1 shows peaks that correspond to the (111), (200), (220), and (311) planes of face-centered cubic Ag (JCPDS card no. 00-087-0719). The XRD analysis confirms the crystalline nature of the Ag: NiO nanocomposite (NC), with no additional peaks, indicating that only NiO and Ag are present. The data successfully confirms the synthesis of the Ag: NiO NC. The Scherrer equation was used to estimate the average crystallite size of the Ag: NiO NC, which was found to be approximately 30 nm.

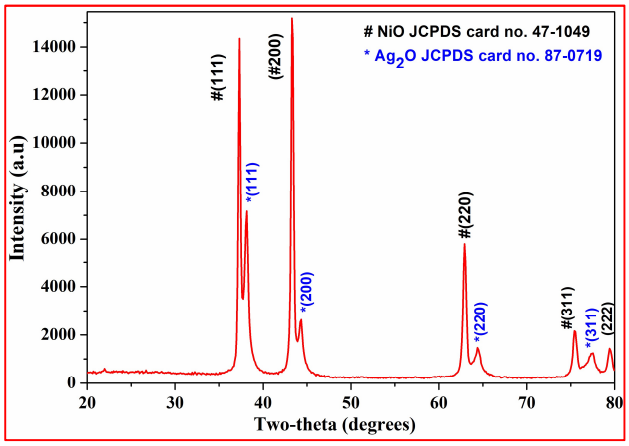

Fig.-1: XRD Spectra of Ag: NiO NC

SEM Analysis

SEM analysis was used to quantify the physical features and investigate the surface morphology and Ag distribution throughout the NiO surface. NiO surfaces have a porous flower-like shape, as seen in Fig.-2, and loading Ag into the pores of NiO does not substantially alter its morphology. The SEM image in Fig.-2 showed that NiO nanostructures had a hexagonal shape and an average particle size of about 85 nm. The above results show that these are compositions of Ag and NiO.

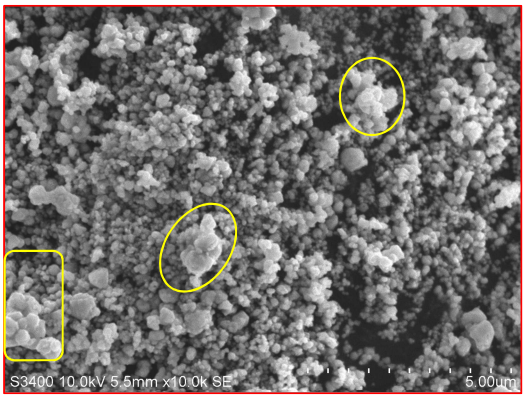

Fig.-2: SEM Image of Ag: NiO NC

EDAX Analysis

The chemical composition of a sample was measured by the EDAX method. The presence of Ag in the modified NiO nanoparticle, together with the fundamental components Ni and O, is confirmed in Fig.-3. Ag's existence across the NiO host structure's surface is strongly supported by the occurrence of different signals that correspond to these elements. The elemental mapping for Ni, O, and Ag in Fig.-3 indicates the presence of the corresponding Ag: NiO NC.[42]

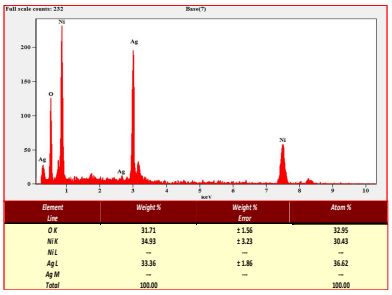

Fig.-3: EDAX Spectra of Ag: NiO NC

TEM Analysis

TEM was used to obtain profound insights into the structure and morphology of the developed materials. The TEM image in Fig.-4(a-b and c) confirmed the presence of two phases, i.e., NiO and Ag, in 5 µm and 500 nm magnifications, revealing structures that were face-centered cubic and cubic. Lattice fringes between 0.21 and 0.24 nm in spacing are visible in the TEM picture in Fig.-4(a-b), which corresponds to the (200) and (111) planes of NiO and Ag, respectively.[39,45] The effective synthesis of Ag: NiO NC is confirmed by the microscope results, which agree well with the XRD data. The TEM image clearly shows the highly agglomerated particle structure, a characteristic of products that are produced by combustion. The SAED pattern is characterized by a unique ring Fig.-4(d). The diffraction spots or rings that correspond to both the Ag and NiO phases, confirming their crystalline nature. Ag diffraction spots typically correspond to the FCC structure, while NiO shows diffraction rings/spots consistent with its cubic structure.

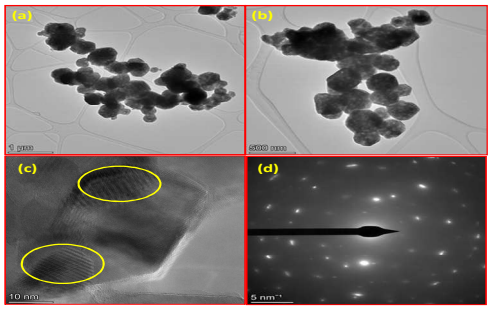

Fig.-4: (a-c) TEM Analysis of Ag: NiO NC in Various Magnifications, (d) SAED Spectral Analysis

DRS Analysis (UV)

Figure-5(a) shows the absorbance in the UV region of Ag: NiO NC. The energy band gap was calculated by using eq.-3.

$$E = hc/\lambda \qquad (3)$$

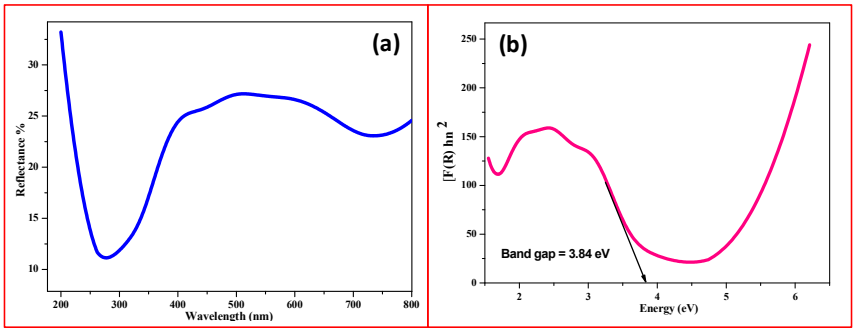

Fig.-5: (a) UV Spectra of Ag: NiO NC, (b) Energy Bandgap of Ag: NiO NC

The UV spectra clearly show that the Ag: NiO NC exhibits a band gap value of 3.84 eV for consistent with previous research on Ag-NiO.[43] Figure-5(b). The absorbance edge of the Ag: NiO nanocomposite (NC) was observed at a lower energy. The unique characteristics of the Ag: NiO NC are attributed to the interfacial electrical interaction between Ag and NiO. Specifically, the electron-electron repulsion in NiO,

facilitated through O 2p orbitals, increases the valence band potential of NiO, resulting in a reduction of the overall band gap.[43]

TGA Analysis

The thermal stability of the synthesized Ag: NiO nanocomposite (NC) was evaluated using thermogravimetric analysis (TGA) under a nitrogen atmosphere, with temperatures ranging from 20 to 800 °C, as shown in Fig.-6. The figure reveals two stages of weight loss, with a gradual decrease in weight from the initial temperature up to 800 °C. The total weight loss observed was 8.86%. The first weight loss of 3.71% occurred between ambient temperature and 190 °C, corresponding to the evaporation of water molecules during crystallization, which is linked to a small endothermic peak at 145 °C. The second weight loss of 5.15% occurred between 190 and 800 °C, indicating the decomposition of organic molecules present in the synthesized material during the green synthesis process. Broad endothermic peaks between 140 and 800 °C were attributed to the decomposition of nitrate compounds in the precursor material. After these two stages of weight loss, the TGA curve shows no further significant weight reduction, indicating the Ag: NiO nanocomposite's excellent thermal stability and 90.81% residual mass. Based on the TGA analysis, the study confirms the use of 400 °C as the calcination temperature for the synthesis of Ag: NiO nanocomposites, consistent with the literature on the calcination temperatures for Ag: NiO nanoparticles.

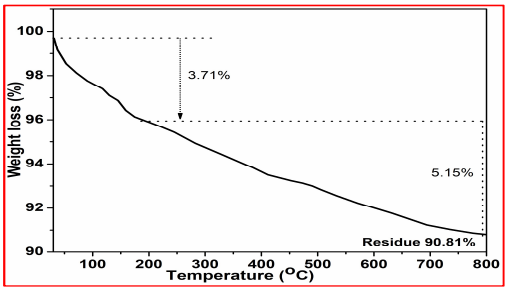

Fig.-6: TGA Spectra of Ag: NiO NC

Photocatalytic Activity

The photocatalytic properties of the synthesized NC were demonstrated using an anionic organic dye. The PCA of the Ag: NiO NC was assessed by the time interval of 0 to 120 minutes for the photodegradation of FOR, with a maximum absorption observed at 495 nm in the UV region Fig.-7[7]**.** The Fig.-7 clearly shows that as the period increases, the absorption value decreases, confirming that the catalytic role is important for the degradation of the FOR dye under UV light.

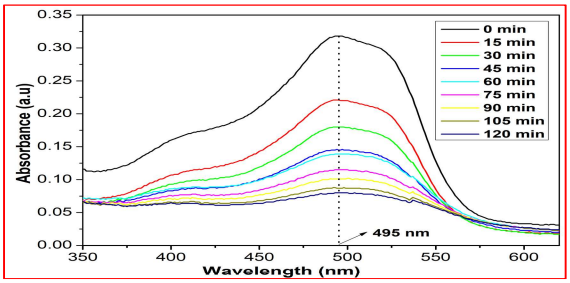

Fig.-7: Photocatalytic Activity of FOR Degradation Under UV Light Irradiation

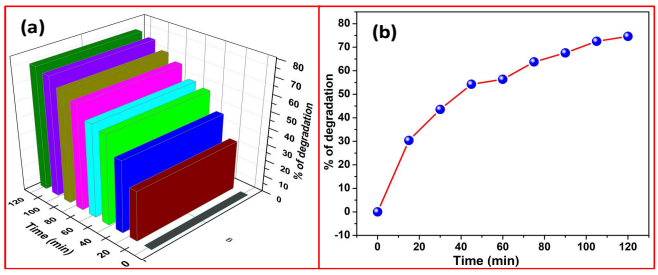

Fig.-8: (a and b) Percentage of Degradation vs Time

Figure-8(a and b) shows an increase in percentage of degradation from 0 to 120 min of UV exposure; the photodegradation rate of FOR dye increased to 74.59% in UV. This demonstrates that when exposed to UV light, Ag: NiO NC has stronger photocatalytic behavior as a catalyst in the degradation of FOR dye.

Kinetic Studies

The kinetics modeling was carried out using 50 mL of dye solution with a beginning concentration of 2.2 × 10 mol. L^{-1}. The thin film was then contacted following regular intervals of irradiation at room temperature. This kinetics method was analyzed by the pseudo-first-order equation.[46] The Ag: NiO NCs PCA progressively increases under UV light irradiation, reaching after 120 minutes. The C/Co equilibrium values showed that pristine NiO had a much lower C/Co value than Ag: NiO NC, indicating that the inclusion of silver dopants enhanced photocatalytic performance Fig.-9(a and b). These results are in line with earlier research showing a link between higher photocatalytic activity and lower optical band gap energies.[39] In this study, the electrical interaction among NiO and dye molecules was improved as a result of the band gap reduction.

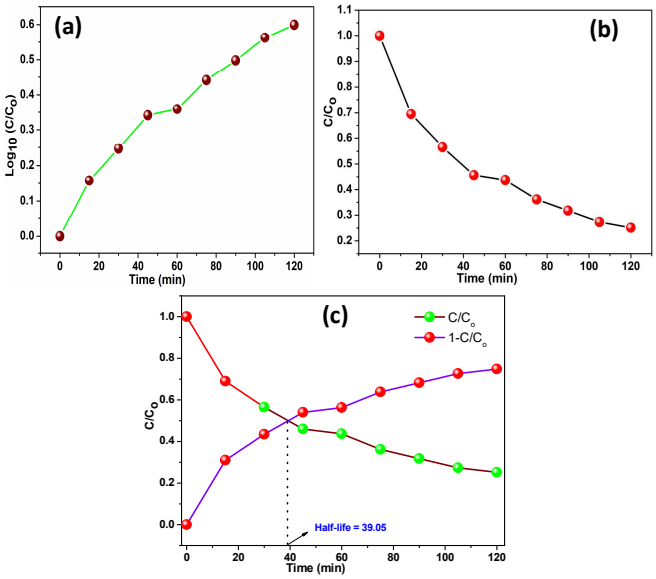

Fig.-9: Kinetic Studies of Ag: NiO NC

Charge transmission from the catalyst to the Fermi level of the dye molecules was made easier by a smaller band gap, which improved the transfer of charge from the valence band to the conduction band. As a result, the catalyst's surface experienced an increase in dye molecule adsorption, which improved the efficiency of degradation.[44] The obtained results show that the photocatalytic degradation of FOR is considerably influenced by the addition of Ag dopant to NiO thin films. The kapp values increase as the Ag dopant content increases in the context of FOR deterioration.

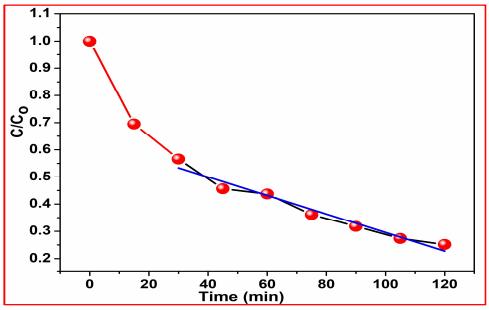

Fig.-10: The Plot of Pseudo-First-Order Kinetics of Ag: NiO NC

This implies that photocatalytic activity is enhanced by the presence of Ag in the NiO lattice, resulting in a faster rate of degradation. A decrease in the band gap is the cause of this increase in the rate constant.[47] More electron and/or hole trapping sites are made available by the addition of Ag ions, which improves

FOR degradation and increases the production of reactive oxidative species. These results advance our knowledge of the fundamental chemistry behind the use of doped semiconductor materials for the photocatalytic destruction of organic contaminants. Figure-9(c) illustrates a clear decrease in the concentration of FOR dyes (C/C_0) with increasing irradiation time. After 120 minutes of photo irradiation, a decrease in the dye concentrations of FOR from 1.0 to 0.49 was observed. The half-life period of Ag: NiO NC was 39.05.

The dye degradation rate was also used to assess the Ag: NiO NC catalyst's photocatalytic performance. The degrading reaction's pseudo-first-order kinetics was shown as a straight line from a plot of C/C_0 v/s time in Fig.-10. A rate constant (k_1) of 0.00342 min^{-1}(R^2 = 0.9541) for FOR was observed from a slope of the graph.

Mechanism

The degradation of FOR dye occurs through a photocatalytic process triggered by light, which involves several chemical reactions. Initially, the surface of the Ag-NiO photocatalyst becomes coated with the FOR dye. When dye molecules are brought close to light, they undergo excitation and generate pairs of electrons, producing a highly active species on the Ag-NiO photocatalyst's surface. The oxidation and reduction processes involve both electrons and holes. Holes oxidize water molecules, generating hydroxyl radicals, while electrons reduce molecular oxygen, forming superoxide radicals. When these hydroxyl and superoxide radicals interact with the FOR dye, they break the chemical bonds within the dye Scheme-2. Equations 4–and 10 illustrate the proposed reaction mechanism for the degradation of FOR dye mediated by the Ag: NiO NC photocatalyst.

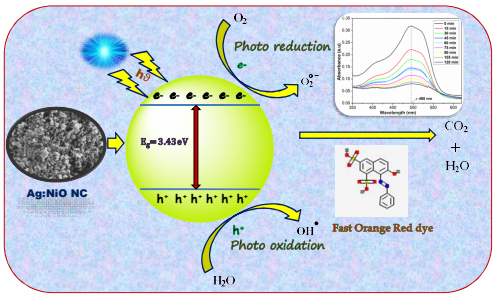

Scheme-2: Graphical Representation of Photo-Degradation of FOR Dye

Ag:NiO NC + hν → Ag:NiO NC (e_{CB}^- + h_{VB}^+)	(4)
$H_2O + H^+ \rightarrow OH^* + H^+$	(5)
$OH^- + h^+ \rightarrow OH^*$ (hydroxyl radical)	(6)
$O_2 + e^- \rightarrow O_2^{*-}$ (superoxide anion)	(7)
$O_2^{*-} + H^+ \rightarrow OH^*$	(8)
FOR + OH^* → Oxidation Product	(9)
FOR + h^+ → Oxidation of FOR	(10)

Electrochemical Investigation

The electrochemical response of the Ag: NiO NC electrode in a 1 M KOH electrolyte was evaluated using Galvanostatic Charge-Discharge (GCD), Electrochemical Impedance Spectroscopy (EIS), and Cyclic Voltammetry (CV). A three-electrode system was employed for the electrochemical measurements. Figure-11(a) presents the CV curves of the Ag: NiO NC electrode at different scan rates of 10, 20, 30, 40, and 50 mV/s, with the voltage window spanning from 0.6 to -0.6 V (vs. Ag/AgCl). The data indicate that the use of an Ag: NiO NC electrode produced a unique behavior. The increase in scan rate is shown by the redox peak, which emerged at -0.01 V (cathodic) and -0.30 V (anodic) at 10 mV/s. This redox behavior was thought to be caused by the reduction (cathodic, discharging) of NiOOH to NiO and the oxidation (anodic, charging) of NiO to NiOOH.[41]

The CV curves clearly show a pair of strong redox peaks related to the Faradaic redox reactions associated with the surface redox mechanism of Ni^{2+} to Ni^{3+}, which exhibits the electrode's pseudocapacitance characteristics. The following is a description of the potential redox reaction.[41]

$$NiO + OH^- \leftrightarrow NiOOH + e^-$$

It is clear that the appearance of CV curves does not significantly alter as scan rates increase, indicating the high-rate performance, rapid electron conduction in the Ag: NiO NC network topologies, and good kinetic reversibility of the Ag: NiO NC electrode. The peak currents for oxidation and reduction enhanced in a linear fashion using the square root of the scan rate vs I_p (Fig.-11(b)), characterized by y =0.007(μM)+0.0060, R^2= 0.9368.

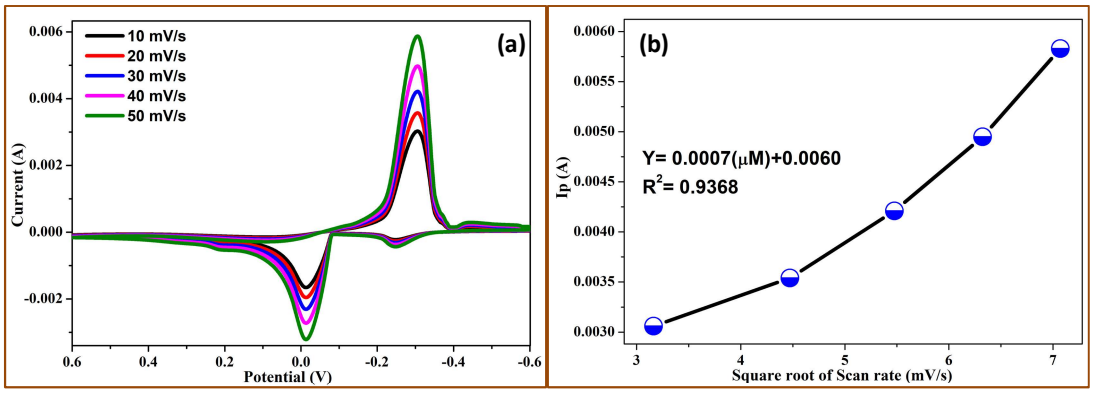

Fig.-11: (a) The CV Studies of the Prepared Electrode and its Variation in the Scan Rate. (b) Calibration Curve

Galvanostatic Charge–Discharge

Figure-12(a) displays the GCD curves of the Ag: NiO NC electrode at varying discharge current densities of 1, 2, 3, 4, and 5 A/g. The pseudocapacitive behavior of the Ag: NiO NC electrode is further confirmed by the nonlinear charge-discharge curves. The specific capacitances (C, F/g) were calculated using the following eq.-11.[48]

$$CA = I\Delta t/A\Delta v \quad (11)$$

Where the discharge current, discharge time, electrode material mass, and voltage interval are denoted by I (A), Δt (s), m (g), and Δv (V), respectively. Table-1 displays the Ag: NiO NC electrode's computed specific capacitances.

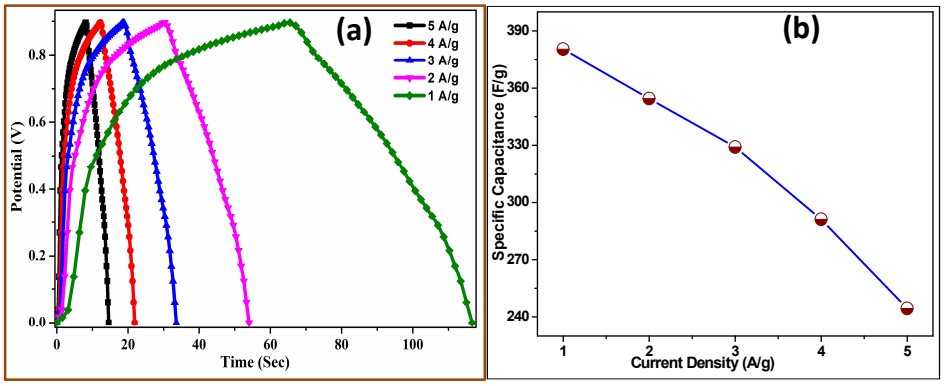

Fig.-12: (a) GCD Curves of Ag: NiO NC Electrode at Current Densities Varying from 1 to 5 A/g. (b) Specific Capacitance vs Current Density Plot

Table-1: Specific Capacitance Vs Current Density

Current density (A/g)	Specific Capacitance (F/g)
1	380.4
2	354.5
3	329.1
4	291.2
5	244.4

The direct growth of Ag: NiO NC electrode materials on the nickel foam substrate with lower resistance and the distinctive Ag-doped NiO structure of networks are thought to be the causes of this outstanding electrochemical performance. In particular, the direct growth of Ni foam electrode materials prevents the

"dead surface" and facilitates effective charge exchange. Electrochemical performance is enhanced by these interconnected Ag: NiO NC network structures, which contain huge amounts of superfine nanowires that are highly conductive to promote the diffusion of electrolyte ions and carry electrons. The electrolyte penetration inside electrode materials may be facilitated by the mesoporous structure of Ag: NiO NC. Furthermore, the conductivity of the Ag: NiO NC electrode material is improved by Ag doping.
The Ag: NiO NC electrode's specific capacitance change at various current densities is shown in Fig.-12(b). The comparatively adequate active substance and ionic rate of diffusion involved in the faradaic redox mechanism at higher current densities are responsible for the observed increase in specific capacitance with increasing current density. Investigating the electrode's long-term cycle stability is essential for supercapacitor practical applications.

EIS Analysis

The purpose of the EIS was to measure the Ag: NiO NC's charge efficiency Fig.-13. In an EIS plot, the resistance of the galvanic system (Rs) is represented by the intercept of the curve on the real Z axis at high frequencies, while the charge-transfer resistance (Rct) is indicated by the diameter of the semicircle. At lower frequencies, the slope of the curve reflects ion diffusion. The Nyquist plot for the Ag: NiO NC electrode exhibited a low charge-transfer resistance, suggesting strong conductivity, as shown in Fig.-13. As reported in previous studies, the Ag: NiO NC electrode demonstrated reduced Rct and Rs, which is attributed to the insertion of Ag, providing a fast electron transport pathway that enhances the electrochemical reaction performance.[43]

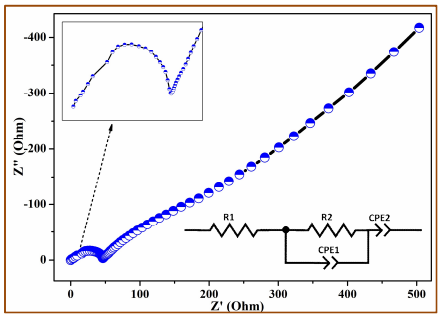

Fig.-13: Nyquist Plot of Ag: NiO NC (insert an equivalent circuit)

Improved electrochemical charge storage performance was demonstrated by the Ag: NiO NC. It was thought that the addition of Ag to the synthesized NC would provide quick electrical channels for electrochemical performance.[49] This is explained by the reduction in internal resistance of the Ag: NiO NC electrode.[43] The superior electrical conductivity of Ag due to its metallic character promotes improved transport of electrons in Ag-NiO NC. The electron journey between NiO and the current collector was thought to be improved by this. Ag NPs' conductive channel contributes to increased charge efficiency, higher material usage, and ultimately improved electrochemical performance by advancing redox processes.[43]

Stability Analysis

The GCD curves for an Ag: NiO NC electrode at a current density of 5 Ag^{-1} are shown in Fig.-14. In a potential range of 0 to 0.8 V, the electrode was monitored over 3000 cycles in relation to Ag/AgCl. The purpose of the research was to ascertain how durable the electrodes were. When compared to the other electrodes, the Ag: NiO NC electrode exhibits superior cycle stability as shown in Fig.-14.
A series of 25-cycle CV scans were performed on the Ag: NiO NC sample at a scanning rate of 50 mVs^{-1} to comprehend the electrode stability of the developed oxides (Fig.-15(a)). There is no discernible variation in the anodic and cathodic peak positions of the electrode with increasing cycles, indicating good electrode stability. Figure-15(b) displays the Ag: NiO NC electrode's 3000 continuous charge-discharge evaluation at a high current density of 5 Ag^{-1}. As the number of cycles increases, the specific capacitance value remains constant until 2300 cycles, after which it slightly decreases at 2800 cycles and then nearly stays the same for the remaining cycles. The synthesized Ag: NiO NC electrode has

outstanding cycle stability, retaining 94.5% of its starting value after 3000 cycles. This suggests that the electrode is appropriate for use in supercapacitors.

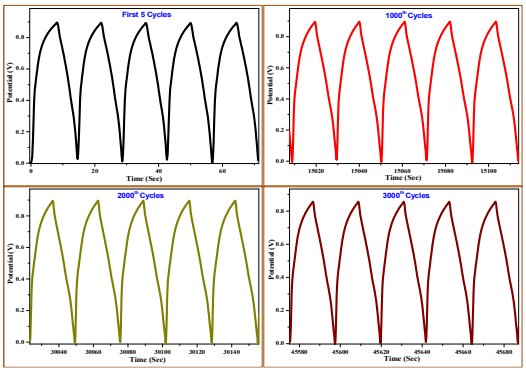

Fig.-14: Galvanostatic Charge-Discharge Curve 1st 5, 1000th, 2000th and 2000th Cycles of Ag:NiO NC Electrode

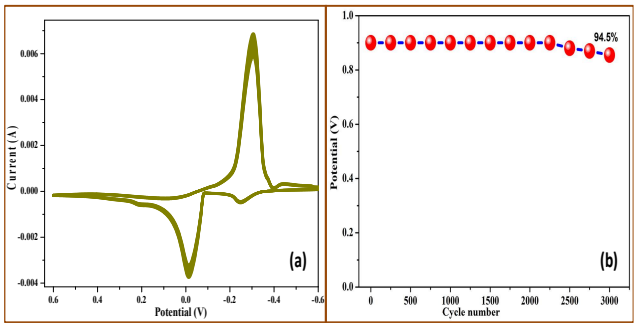

Fig.-15: (a) CV Scans of 25 Cycles, at a Scanning Rate of 50 mVs$^{-1;}$ (b) Number of Cycles of Ag: NiO NC Electrodes at a Current Density of 5 Ag^{-1}

CONCLUSION

The Ag: NiO nanocomposite was synthesized through a biomediated solution combustion method using Tulsi leaf extract. The confirmation of the Composite material is done by various spectral investigation methods. The XRD shows the average crystallite size of Ag: NiO NC is ~ 30 nm. SEM shows a hexagonal shape with an average particle size of 85 nm. The TEM images show that Ag diffraction spots typically correspond to the FCC structure, while NiO corresponds cubic structure. The energy band gap value for Ag: NiO NC of 3.84 eV is confirmed by DRS spectra. The TGA shows good heat stability and 90.81% of residue formation with calcination temperature developed even after 400 °C. The photodegradation of Fast Orange Red (FOR) shows a maximum absorption observed at 495 nm with 74.59% degradation under UV light irradiation. The Cyclic Voltammetric (CV) studies exhibit a surface redox mechanism of Ni^{2+} to Ni^{3+}, which emerged at -0.01 V (cathodic) and -0.30 V (anodic) at 10 mV/s using 1 M KOH solution. The GCD confirms good specific capacitances of 380.4 F/g at a current density of 5 A/g. The Ag: NiO NC shows outstanding cycle stability, retaining 94.5% of its starting value after 3000 cycles. This suggests that the electrode is appropriate for use in supercapacitors.

ACKNOWLEDGEMENTS

Authors are thankful to the authorities of their institutions for providing the basic facilities for this research.

CONFLICT OF INTERESTS

The authors declare that there is no conflict of interest.

AUTHOR CONTRIBUTIONS

The present work is related to *SDG-3: Good Health and Well-being*. All the authors contributed significantly to this manuscript, participated in reviewing/editing and approved the final draft for publication. The research profile of the authors can be verified from their ORCID ids, given below:

Ramasubbaiah Vusenappagari https://orcid.org/0009-0001-9415-6924
Behara Dilip Kumar https://orcid.org/0000-0002-4005-7234

Open Access: This article is distributed under the terms of the Creative Commons Attribution 4.0 International License (http://creativecommons.org/licenses/by/4.0/), which permits unrestricted use, distribution, and reproduction in any medium, provided you give appropriate credit to the original author(s) and the source, provide a link to the Creative Commons license, and indicate if changes were made.

REFERENCES

1. Z. Carmen, S. Daniel, *Environmental and Analytical Update*, *T. Puzyn, Ed., InTech Book* (2012), https://doi.org/10.5772/32373
2. S.D. Melvin, F.D.L. Leusch, *Environment International,* **92–93**, 183(2016), https://doi.org/10.1016/j.envint.2016.03.031
3. M.H. Habibi, E. Shojaee, *Spectrochimica Acta Part A*: *Molecular and Biomolecular Spectroscopy,* **229**, 117796(2020), https://doi.org/10.1016/j.saa.2019.117796
4. R. Ranjitha, K.N. Meghana, V.G. Dileep Kumar, Aarti S. Bhatt, B. K. Jayanna, C.R. Ravikumar, Mysore Sridhar Santosh, H. Madhyastha, K. Sakai, *New Journal of Chemistry*, **45(2)**, 796(2021), https://doi.org/10.1039/D0NJ05268J
5. Iqra Rabani, Chinna Bathula, Rabia Zafar, Gul Zari Rabani, Sajjad Hussain, Supriya A. Patil, Young Soo Seo, *Journal of Environmental Chemical Engineering,* **9**, 104852(2021), https://doi.org/10.1016/j.jece.2020.104852
6. N. Nasir Ahamed, Jayadev Pattar, V.G. Dileep Kumar, T. Naveen Kumar, N. Basavaraju, T.M Sharanakumar, C.R. Ravikumar, *Analytical Chemistry Letters,* **14(3)**, 269(2024), https://doi.org/10.1080/22297928.2024.2361788
7. R. Lakshmana Naik R, T. Bala Narsaiah, P. Justin, M. Dhanalakshmi, A. Naveen Kumar, M.N. Somashekar, T.M. Sharanakumar, C.R. Ravikumar, H.C. Ananda Murthy, *Journal of the Indian Chemical Society,* **101(10)**, 101247(2024), https://doi.org/10.1016/j.jics.2024.101247
8. Nishath Afza, M. S. Shivakumar, M. Mylarappa, S. Anil Subash, C. R. Ravikumar, T. M. Sharanakumar, M. N. Somashekar, *Electrocatalysis,* **16**, 78(2025), https://doi.org/10.1007/s12678-024-00898-3
9. M.N. Somashekar, M. Dhanalakshmi, T.S. Nagamani, T. Subhas Chandra, T.M. Sharanakumar, C.R. Ravikumar, *Sensors International,* **6**, 100308(2025), https://doi.org/10.1016/j.sintl.2024.100308
10. R. Lakshmana Naik, T. Bala Narsaiah, P. Justin, H. N. Shwetha, T. M. Sharanakuamr, M. N. Somashekar, C. R. Ravikumar and Apsar Pasha, *Research on Chemical Intermediates,* **51(2)**, 1093(2025), https://doi.org/10.1007/s11164-024-05468-2
11. Aida Garcia-Rodríguez, Víctor Matamoros, Clàudia Fontàs, Victòria Salvadó, *Environmental Science and Pollution Research,* **21(20)**, 11708(2014), https://doi.org/10.1007/s11356-013-2448-5
12. Mir Sayed Shah Danish, Liezel L. Estrella, Ivy Michelle A. Alemaida, Anton Lisin, Nikita Moiseev, Mikaeel Ahmadi, Massoma Nazari, Mohebullah Wali, Ameedullah Zaheb, Tomonobu Senjyu, *Metals*, **11**, 80(2021), https://doi.org/10.3390/met11010080
13. Arindam Dutta, Shirsendu Mitra, Mitali Basak, Tamal Banerjee, *Energy Storage*, **5(1)**, e339(2023), https://doi.org/10.1002/est2.339
14. Oluwaseye Samson Adedoja, Emmanuel Rotimi Sadiku, Yskandar Hamam, *Polymers*, **15(10)**, 2272(2023), https://doi.org/10.3390/polym15102272
15. R.B. Rajput, S.N. Jamble, R. B. Kale, *Journal of Environmental Management,* **307**, 114533(2022), https://doi.org/10.1016/j.jenvman.2022.114533
16. Rosana A. Gonçalves, Rosimara P. Toledo, Nirav Joshi, Olivia M. Berengue, *Molecules,* **26(8)**, 2236(2021), https://doi.org/10.3390/molecules26082236
17. Xueqin Liu, James Iocozzia, Yang Wang, Xun Cui, Yihuang Chen, Shiqiang Zhao, Zhen Li, Zhiqun Lin, *Energy and Environmental Science* **10**, 402(2017), https://doi.org/10.1039/C6EE02265K
18. Aminuddin Bin Ahmad Kayani, Sruthi Kuriakose, Mahta Monshipouri, Fararishah Abdul Khalid, Sumeet Walia, Sharath Sriram, Madhu Bhaskaran, *Nano Micro Small,* **17(32)**, 2100621(2021), https://doi.org/10.1002/smll.202100621

19. Noorah A Al-Ahmadi, Materials Research Express, *Materials Research Express*, **7,** 032001(2020), https://doi.org/10.1088/2053-1591/ab7a60
20. Mohammad Ehtisham Khan, Akbar Mohammad, Wahid Ali, Abdulrahman Ahmed Sharwani, *Inorganic Anticorrosive Materials,* pp.95-111(2022), https://doi.org/10.1016/B978-0-323-90410-0.00006-4
21. A. Dey, *Materials Science and Engineering*: B, **229**, 206(2018), https://doi.org/10.1016/j.mseb.2017.12.036
22. Usman Qumar, Jahan Zeb Hassan, Rukhsar Ahmad Bhatti, Ali Raza, Ghazanfar Nazir, Walid Nabgan, Muhammad Ikram, *Journal of Materials Science and Technology,* **131**, 122(2022), https://doi.org/10.1016/j.jmst.2022.05.020
23. Gang Nie, Yu Yao, Xiaoguang Duan, Ling Xiao, Shaobin Wang, *Current Opinion in Chemical Engineering,* **33**, 100693(2021), https://doi.org/10.1016/j.coche.2021.100693
24. Ruibin Liang, Yongquan Du, Peng Xiao, Junyang Cheng, Shengjin Yuan, Yonglong Chen, Jian Yuan, Jianwen Chen, *Nanomaterials,* **11(5)**, 1248(2021), https://doi.org/10.3390/nano11051248
25. Gianluca Fiori, Francesco Bonaccorso, Giuseppe Iannaccone, Tomás Palacios, Daniel Neumaier, Alan Seabaugh, Sanjay K. Banerjee, Luigi Colombo, *Nature Nanotech*, **9,** 768(2014), https://doi.org/10.1038/nnano.2014.207
26. Yanchun Yang, Yinghui Han, Wenkun Jiang, Yuyang Zhang, Yanmei Xu, Ayman Mahmoud Ahmed, *Applied Science*, **12(1)**, 354(2022), https://doi.org/10.3390/app12010354
27. P.C. Nagajyothi, S.V. Prabhakar Vattikuti, K.C. Devarayapalli, K. Yoo,Jaesool Shim, T.V.M. Sreekanth, *Critical Reviews in Environmental Science and Technology,* **50(24)**, 2617(2020), https://doi.org/10.1080/10643389.2019.1705103
28. Maria P. Nikolova, Murthy S. Chavali, *Biomimetics*, **5(2)**, 27(2020), https://doi.org/10.3390/biomimetics5020027
29. D. Kishore Kumar, Jan Kříž, N. Bennett, Baixin Chen, H. Upadhayaya, Kakarla Raghava Reddy, Veera Sadhu, *Materials Science for Energy Technologies,* **3**, 472(2020), https://doi.org/10.1016/j.mset.2020.03.003
30. Wei Wu, Man Wang, Jianmin Ma, Yuliang Cao, Yonghong Deng, *Advanced Electronic Materials,* **4(8)**, 1800185(2018), https://doi.org/10.1002/aelm.201800185
31. Yingqi Jiang, Pengbo Wang, Xining Zang, Yang Yang, Alina Kozinda, Liwei Lin *Nano Letters*, Nano Lett, **13(8)**, 3524(2013), https://doi.org/10.1021/nl400921p
32. V. Bhoomika, N. Basavaraju, K.T. Monalisa, Syed Khasim, T.R. Shashi Shekhar, T.M. Sharanakuamr, H.C. Ananda Murthy, C.R. Ravikumar, *Results in Chemistry*, **13,** 101924, (2025). https://doi.org/10.1016/j.rechem.2024.101924
33. A. Almatroudi, *Open Life Sciences,* **15(1)**, 819(2020), https://doi.org/10.1515/biol-2020-0094
34. Y. Zheng, A. Wang, *Journal of Materials Chemistry,* **22(32)**, 16552(2012), https://doi.org/10.1039/C2JM32774K
35. Saba Hemmati, Majid M. Heravi, Bikash Karmakar, Hojat Veisi *Journal of Molecular Liquids,* **319**, 114302(2020), https://doi.org/10.1016/j.molliq.2020.114302
36. Lu Han, Cheng-Mei Liu, Shi-Lei Dong, Cai-Xia Du, Xiao-Yong Zhang, Lu-Hai Li, Yen Wei, *Biosensors and Bioelectronics,* **87**, 466(2017), https://doi.org/10.1016/j.bios.2016.08.004
37. Lu Zheng, Gaini Zhang, Miao Zhang, Shaohua Guo, Zong–Huai Liu, *Journal of Power Sources,* **201**, 376(2012), https://doi.org/10.1016/j.jpowsour.2011.11.026
38. Nagi M. El-Shafai, Mustafa Shukry, Swellam W. Sharshir, Mohamed S. Ramadan, A. Alhadhrami, Ibrahim El-Mehasseb, *Journal of Energy Storage,* **50**, 104626(2022); https://doi.org/10.1016/j.est.2022.104626
39. Saravanakumar Karunamoorthy, Muthuraj Velluchamy, *Journal of Materials Science,* **29**, 20367(2018), https://doi.org/10.1007/s10854-018-0172-0
40. Sadayappan Nagamuthu, Kwang-Sun Ryu, *Scientific Reports*, **9**, 4864(2019), https://doi.org/10.1038/s41598-019-41446-0

41. Shahid Hussain, Piaopiao Wan, Nimra Aslam, Guanjun Qiao, Guiwu Liu, Mingsong Wang, *Journal of Materials Science: Materials in Electronics,* **29(3)**, 1759(2018), https://doi.org/10.1007/s10854-017-8084-y
42. Karuppiah Chinnaiah, Karthik Kannan, Nadezhda Palko, Maria Grishina, L. Guganathan, Krishnamoorthy Gurushankar, *Ionics,* **30**, 1691(2024), https://doi.org/10.1007/s11581-023-05361-9
43. Chaitali V. Khedkar, Amol S. Vedpathak, Abhijeet V. Dhotre, Krishna D. Daware, Yesh D. Kolekar, Shrikrishna D. Sartale, Suresh W. Gosavi, Shankar I. Patil, *Chemical Physics Impact,* **6**, 100153(2023), https://doi.org/10.1016/j.chphi.2022.100153
44. S Sid Ahmed Benseghier, Farid Bennabi, Ismail Ercan, Hamid Nehmar, Yasmina Khane, Nasreddine Moulayat, Filiz Ercan, Tarek Kayed, Mehdi Adjdir, *Inorganic Chemistry Communications,* **159**, 111787(2024), https://doi.org/10.1016/j.inoche.2023.111787
45. Suresh Kumar Pandey, Manish Kumar Tripathi, V. Ramanathan, Pradeep Kumar Mishra, Dhanesh Tiwary, *Journal of Physics and Chemistry of Solids,* **159**, 110287(2021), https://doi.org/10.1016/j.jpcs.2021.110287
46. Mir Waqas Alam, V.G. Dileep Kumar, C.R. Ravikumar, S.C. Prashantha, H.C. Ananda Murthy, M.R. Anil Kumar, *Journal of Physics and Chemistry of Solids,* **161**, 110491(2022), https://doi.org/10.1016/j.jpcs.2021.110491
47. S. Karunamoorthy, M. Velluchamy, *Journal of Materials Science: Materials in Electronics,* **29(23)**, 20367(2018); https://doi.org/10.1007/s10854-018-0172-0
48. R. Lakshmana Naik, T. Bala Narsaiah, *Materials Today: Proceedings,* **72**, 268(2023), https://doi.org/10.1016/j.matpr.2022.07.266
49. Wenbo Zhu, Panpan Wang, Zhe Chen, Chengyan Xu, Yan Jiao, Mingyu Li, Yan Huang, *Journal of Materials Chemistry A*, **10**, 10780(2022), https://doi.org/10.1039/D2TA01024K

[RJC-9320/2025]